IEEE Access
Multidisciplinary ⋮ Rapid Review ⋮ Open Access Journal

Received November 25, 2021, accepted December 20, 2021, date of publication December 24, 2021,
date of current version December 31, 2021.

Digital Object Identifier 10.1109/ACCESS.2021.3138563

Measurement-Based Outage Probability Estimation for Mission-Critical Services

MELISA LÓPEZ[1], (Graduate Student Member, IEEE), TROELS B. SØRENSEN[1], ISTVÁN Z. KOVÁCS[2], (Member, IEEE), JEROEN WIGARD[2], AND PREBEN MOGENSEN[1,2]

[1]Department of Electronic Systems, Wireless Communication Networks Section, Aalborg University, 9220 Aalborg, Denmark
[2]Nokia, 9220 Aalborg, Denmark

Corresponding author: Melisa López (mll@es.aau.dk)

ABSTRACT An accurate estimation of the service quality that the user will experience along a route can be extremely useful for mission-critical services. Based on availability and reliability estimations, it can provide the network with in-advance information on the potential critical areas along the route. If such estimation is based on empirical/statistical or site-specific estimations, both of which are typically used for cellular network planning, it will lead to significant uncertainty in the estimation, as we demonstrate in this paper. Instead, if estimations are based on previously collected measurements, the uncertainty can be significantly reduced. In this paper, we analyze the achievable accuracy of such a data-driven estimation which aggregates measurements from multiple user equipment (UEs) moving along the same route by averaging the measured signal levels over a route segment. We evaluate the estimation error for both empirical/statistical, site-specific and data-driven estimations for measurements collected in urban areas. Based on the demonstrated advantage of data-driven estimation, and the relevance of including context information that we proved in a previous paper, we discuss and analyze how the estimation error can be reduced even further by predicting the Mean Individual Offset (MIO) that each specific UE will observe with respect to the average. To this end, we propose and evaluate a technique for MIO correction that relies on observing a time series of signal level samples when the UE starts a mission-critical service. By observing 100-300 m of real-time samples along the route results show that the overall estimation error can be reduced from 5-6 dB to 4 dB using MIO correction. Finally, using the obtained results, we illustrate how the signal level estimations can be used to estimate the outage probability along the planned route.

INDEX TERMS RSRP estimation, data-driven estimation, LTE measurements, mission-critical communications, service availability, service reliability.

I. INTRODUCTION

5G New Radio (NR) technology is expected to provide connectivity to a wide variety of services with different Quality of Service (QoS) requirements. For some applications, Key Performance Indicators (KPIs) such as reliability, latency, or data rate may have stringent targets which will be challenging to meet with the existing Radio Resource Management (RRM), QoS, and mobility management procedures in Long Term Evolution (LTE) [1]. These procedures are mostly reactive, i.e. actions against a drop in the signal level or the QoS are taken after the drop has already occurred. Having prior knowledge of the network conditions that the User Equipment (UE) will experience can help to avoid a situation that can be critical for the service requirements to be met. Therefore, recently proposed solutions have adopted predictive algorithms and aim for more proactive management of the network resources [2], [3].

The service could strongly benefit from proactive QoS management in the so-called mission-critical communications, such as Unmanned Aerial Vehicles (UAV) or Vehicle-To-Everything (V2X) over cellular networks. The need for this approach is stated by the 5G Automotive Association (5GAA) in [4] where they present the concept of *predictive QoS*, which consists of in-advance notifications from the network to the UE about predicted changes in the QoS. Furthermore, the Aerial Connectivity Joint Activity (ACJA) presents a two-phase operational context for UAVs in [5]. They propose a planning phase where there is the need to determine RF conditions for the planned path and a flight phase where

The associate editor coordinating the review of this manuscript and approving it for publication was Zihuai Lin.

This work is licensed under a Creative Commons Attribution-NonCommercial-NoDerivatives 4.0 License.
For more information, see https://creativecommons.org/licenses/by-nc-nd/4.0/

constant monitoring of the requirements is performed and used for predictive mechanisms based on real-time radio KPIs. A similar framework could be expected for autonomous driving in the V2X context.

A relevant parameter for RRM decisions, as well as for QoS prediction, is the signal level experienced by a UE, typically expressed using the Reference Signal Received Power (RSRP) [6]. RSRP is a key measure used for several procedures such as cell selection and re-selection, handover, and power control. Therefore, the estimation of the signal level perceived by a UE in a certain area is essential in the process of designing a reliable system. Accurate estimations of RSRP levels that the UE will experience along the path could provide in-advance information on the expected service availability and reliability conditions.

There are well-known techniques for planning and estimating the signal level using empirical or deterministic propagation models. However, as it will be shown in this article, despite the ability of these traditional techniques to characterize the signal level in a particular environment, their accuracy along specific paths is too low for predictive QoS purposes.

A. CONTRIBUTIONS

In [7] a data-driven approach for serving cell signal level estimation was presented. The approach aggregates measurements from UEs in the same location and uses their average as an estimation for that location. The technique is shown to achieve an overall estimation error of 5-6 dB, which can be further reduced to 4 dB if the Mean Individual Offset (MIO) of a specific user with respect to the estimation is corrected. The novel contributions included in this article are the following:

- Quantify the advantage of data-driven estimations over statistical and deterministic techniques. We use two empirical models as well as the estimations provided by a ray-tracing tool to show the improved performance of our approach.
- Propose and evaluate an MIO estimation and correction technique that shows an advantage over the use of context information, using real-time measurements of the UE moving along the path.
- Present a framework that estimates areas with a high probability of signal and service degradation that the UE will experience along a route.

B. RELATED WORK

Different KPIs can be used to estimate the QoS and outage probability depending on the service requirements. However, RSRP is one of the most critical parameters when designing a cellular network. Furthermore, the authors in [8] show that, unlike other KPIs such as Reference Signal Received Quality (RSRQ) or throughput, RSRP remains stable for long periods and can be modeled as time-invariant. This stability motivates the choice of RSRP, as it ensures that the estimation is valid for any time of the day.

Estimating the propagation conditions is a widely studied topic in the literature. Empirical models are a practical approach where measurements are used to develop statistical models of the channel and estimate path loss for a particular type of environment. Although there are different models for the different propagation scenarios, their accuracy in a specific location is compromised by the generalization of the model. For the urban environment, there are well-known empirical path loss models such as COST-231 Walfisch-Ikegami [9], and Okumura-Hata [10]. On the other hand, geometric models rely on physics to compute the dominant and secondary paths of the radio waves propagating through a specific propagation environment. This approach is generally more accurate than the empirical techniques but more computationally complex. A common implementation of this estimation technique is ray-tracing [11].

The computational cost of ray-tracing, and the lack of accuracy of stochastic models, led to the study of new approaches. In recent literature, there has been extensive work on signal level estimation. The authors in [12] characterize the fluctuations of signal strength using a large measurement dataset in roads and cities. They conclude that, for static periods, the RSRP shows fluctuations between 1.8 and 2.2 dB, increasing up to 6 dB when considering mobility. In [13], the authors propose a two-step algorithm (clustering and k-nearest neighbor) to predict an RSRP map using UE measurement reports and show a Mean Absolute Error (MAE) of 3.5 dB.

More complex approaches based on Machine Learning (ML) techniques can also be found in the literature. The work in [14] fuses crow-sourced measurements from LTE users with other context information to build a predictive model that provides a Root Mean Squared Error (RMSE) of 7.4 dB. In [15] the authors present a deep learning approach where they use satellite images to extract the features of the receiver's surrounding environment, obtaining a prediction RMSE of approximately 6 dB. The authors in [16] use a feed-forward Neural Network (NN) for path loss estimation showing an RMSE of 6.3 dB when testing the algorithm over measurements from different scenarios. The work in [17] uses a NN for path loss estimation at different frequencies, resulting in a minimum observed RMSE value of 6 dB. The authors of [18] present path loss prediction using artificial NNs, achieving an RMSE of 7 dB.

The proposed technique in [7] is simple. It exploits UE measurement reports for signal level estimation, providing reasonably improved accuracy compared to the existing traditional and non-traditional techniques, especially after using the techniques presented in this article to correct the MIO of the UE. Unlike the literature mentioned above, the technique in [7] is location-specific, i.e., it provides an estimation of the signal level that the UE will experience in a particular location, regardless of which base station (BS) the UE will connect to along the route. The RSRP estimations are used in this article to estimate the outage probability that a particular mission-critical UE will experience along a specific route.

This type of estimation is not available in the current literature to the best of the authors' knowledge.

The rest of the article is organized as follows. Section II presents our vision on service availability and reliability provisioning for mission-critical communications. In Section III we explain how we have obtained the measurements for the analysis in this article, while Section IV shows a summary of the data-driven estimation approach and results presented in [7] as well as a comparison with the traditional signal level estimation techniques. Section V shows results for MIO correction in the pre-service and on-service stages. In Section VI we exemplify how these estimations can be used to provide information on the outage probability along the route and compare the estimation results with recorded values. Section VII concludes the paper with a summary of the findings.

II. SERVICE RELIABILITY PROVISIONING

The mission-critical communication services will most likely require reliability assurance mechanisms within the cellular network. In this context, we build upon the same architecture as specified for QoS sustainability analytics [19], where the Network Data Analytics Function (NWDAF) can notify an external (third-party) application server when QoS degrades over a path of interest.

The Radio Access Network (RAN) is composed of radio cells in the network and handles all radio interface protocols ensuring a minimum QoS can be delivered to the UEs. The core network configures the RAN cells, the analytics function (e.g., NWDAF), and establishes signaling links to the application server for the specific mission-critical service. The application server is assumed to be able to communicate directly with the application layer in the UE.

In our case, following the structure presented in [5], we further consider a two-stage framework for the addressed mission-critical communication services: a ''pre-service'' and an ''on-service'' stage, as it is shown in Fig. 1. The following explanations can be linked to Fig. 1 through notation $^{(\#)}$.

In the pre-service stage, the application server determines that a UE intends to move along a certain route (e.g., UAV flight or V2X drive)$^{(1)}$ and provides information about the planned movement path to the analytics function$^{(2)}$, which then performs route quality estimations$^{(3)}$. For the route quality estimations, the analytics function can use the measurement-based RSRP estimations, e.g., from all other UEs moving along the same path combined potentially with historical measurement data. The service availability estimation is obtained by considering serving cell RSRP estimations and a certain connectivity threshold. For service reliability, Signal-to-Interference-Ratio (SIR) estimations (assuming interference-limited scenarios) can be obtained based on the RSRP reports for the serving and the strongest neighboring cells and compared with the minimum service requirements. RSRP and SIR are used to estimate QoS metrics such as service availability and service reliability, which help to identify the potential critical communication areas along the planned route of the UE. Next, the analytics function replies to the application server with the corresponding route quality estimations$^{(4)}$, and the application server communicates the decision to the UE application e.g., permission to start the mission along the route. Assuming the answer is positive, the application server informs the analytics function$^{(5)}$ and the UE application$^{(6)}$. The analytics function can optionally trigger the procedure to perform more proactive management of the radio resources along the planned movement path of the UE (e.g., prepare potential serving cells)$^{(7)}$.

The ''on-service'' stage is triggered when the UE starts moving along the planned path$^{(8)}$. Once the UE service is started, the UE reports the measured RSRP values to the RAN$^{(9)}$, which forwards them to the analytics function$^{(10)}$. The analytics function uses these measurement reports to predict the RSRP MIOs for a certain time horizon$^{(11)}$. This allows a more accurate estimation of the service availability and reliability along the route. This information would allow the RAN to take action with regard to critical areas, e.g., activate multi-connectivity or apply interference mitigation techniques before SIR becomes too low, etc. Furthermore, the information could be forwarded to the application server, which could potentially revisit its decision.

III. MEASUREMENT CAMPAIGN

A. MEASUREMENT SETUP

An extensive LTE measurement campaign was carried out in order to evaluate the data-driven approach. This campaign aimed to collect RSRP measurements recorded by multiple UEs in a specific route.

Four commercial phones with a test firmware (QualiPoc©) and a professional radio network scanner (R&S TSME) [21] were used during this measurement campaign. Using a specific firmware to measure the radio KPIs ensured that the recorded data was consistent, calibrated, and reliable. However, it also limited the number of mobile devices and the available vendors that could be used for the campaign. Two Samsung Galaxy S5 ($S5_1$, $S5_2$) and two Samsung Galaxy S9 ($S9_1$, $S9_2$) measured several times the same route in multiple positions and orientations. In this article, we used three different setups (referred to as A, B, and C) to obtain as much UE heterogeneity as possible in terms of experienced signal levels along the route, i.e., to increase variation in the aggregated measurements. Further information on the position and orientation of each of the phones in the different setups can be found in Table 1. The scanner antenna remained in a car-top carrier during the whole measurement campaign, and so did the phones for setups A and B, as shown in Fig. 2. During the recording with setup C, the phones were located inside the car. As it will be further explained in Section IV, the recorded data by each of the UEs is averaged to obtain an estimation.

The antenna patterns of the phones were measured using a multi-probe antenna measurement system [22]. Fig. 3 shows

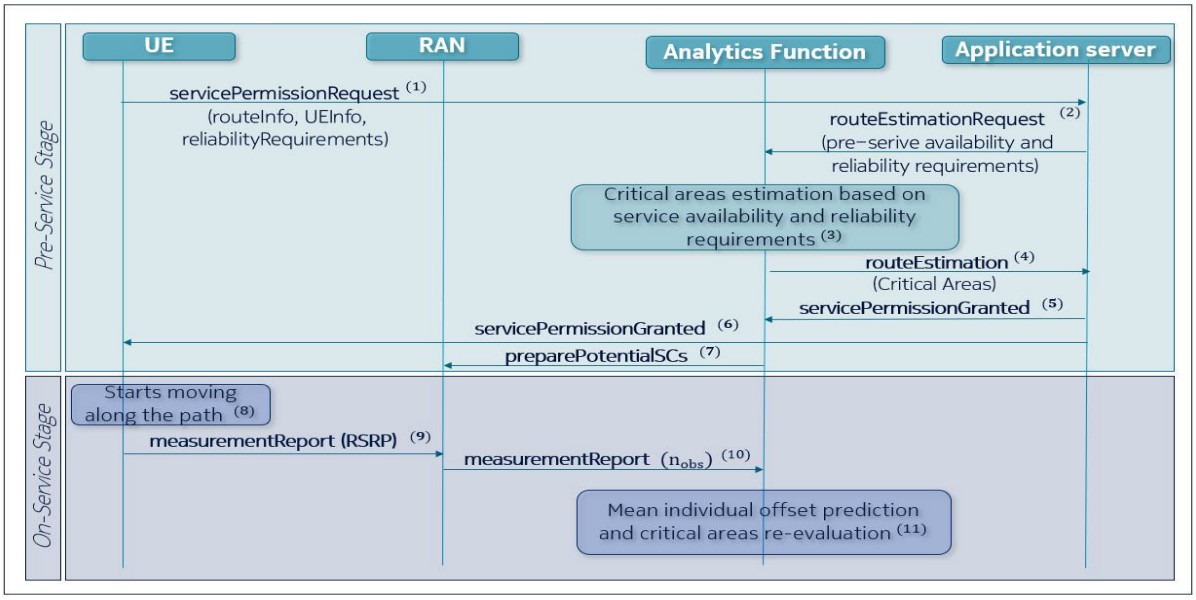

FIGURE 1. Service availability/reliability provisioning scheme.

TABLE 1. Measurement setups information. The IDs can be used as a reference to identify the phones placement in Fig. 2.

ID	Phone	Setup	Position	Orientation
1	$S5_1$	A	Standing	F
2	$S5_2$		Standing	L
3	$S9_1$		Laying	Up
4	$S9_2$		Standing	B
5	$S5_1$	B	Laying	Down
6	$S5_2$		Laying	Up
7	$S9_1$		Laying	Up
8	$S9_2$		Laying	Down
9	$S5_1$	C	Front Seat	L
10	$S5_2$		Glove Compartment	Up
11	$S9_1$		Back Seat	Up
12	$S9_2$		Trunk	Up

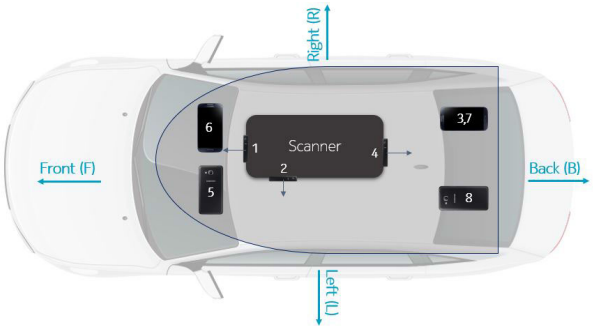

FIGURE 2. Phones placement and orientation in setups A&B in the car top carrier. The numbers in this figure can be mapped to descriptions in Table 1. The radio network scanner is also shown in the center of the car top carrier. For setup C, the phones were located inside the car.

the measured antenna patterns for each of the four phones. As it can be observed, the patterns are similar between the same phone model but significantly different when comparing the S5 and S9 models. As expected, none of them is omnidirectional. The different shapes and orientations of the multiple phones will introduce variation within the traces used to build the serving cell RSRP estimation.

A reference paddle antenna was connected to the radio network scanner and mounted in a fixed position with its main lobe extending towards both sides of the car. This reference was used to exclude the effects of the directional patterns of the phones, allowing us to observe the influence of factors that are inherent to the measurement process, such as changes in the network and/or environment conditions.

In our experimental investigations the UE heterogeneity is achieved through:

- Use of two device models with different chipsets and device antenna implementation (type, placement on the frame, coupling to the frame, etc.), which impact the signal levels observed when the devices are moving.
- Position of the mobile devices with their corresponding directional antenna patterns in different orientations outside the car.
- Location of the mobile devices inside the car in one of the setups, such that the effect of the car body blocking the received signal is also included in the aggregated measurements.

As it is shown in [7], to evaluate the accuracy of the estimation in different environments, data was collected in two scenarios distinguished by completely different characteristics: rural and urban. For the rural case, the car drove 2 round-trips along a 14.8 km stretch with each of the 3 setups, recording RSRP measurements for the two different driving directions. In the urban environment, the route was a 3.3 km loop through which the car drove 3 times with each of the

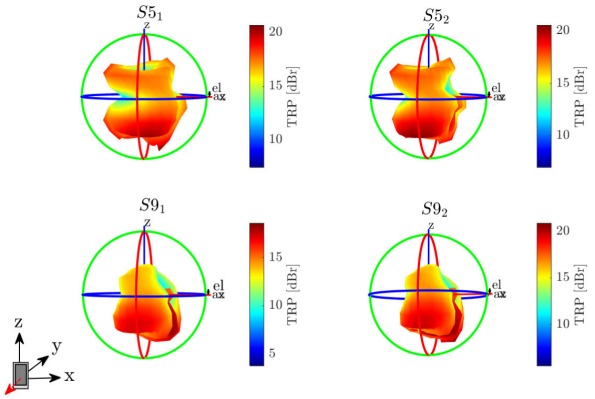

FIGURE 3. Total radiated power (TRP) in dBr (relative) of the measured antenna patterns from the different test phones. The position of the phones in the multi-probe antenna measurement system was along the z-axis with their front (screen) facing against y-axis.

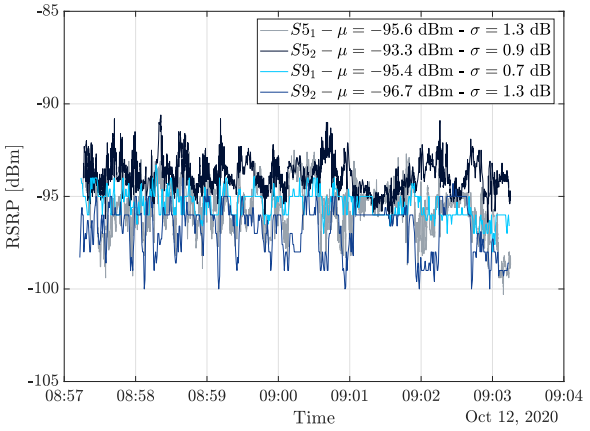

FIGURE 4. Static test of measurement acquisition evaluation. The phones were in the same position and orientation, all connected to the same serving cell.

TABLE 2. Relevant measurement campaign information.

	Rural	Urban
Carrier Frequency	1800 MHz	
Carrier Bandwidth	20 MHz	
RSRP Sampling Rate	500 ms	
Route Length	14.8 km	3 3km
Avg. Driving Speed	65 km/h	22 km/h
Avg. Recorded Samples/10 m	5	8
Coverage	Sparse	Dense
Visibility	Mainly LOS	Mainly NLOS

setups in one direction only due to traffic restrictions. Other relevant information regarding the measurement campaign for the corresponding scenarios can be found in Table 2. For further details, the reader is referred to [7].

B. RSRP RECORDING

The LTE RAN typically configures the UE to report these measurements periodic or event-triggered. The Minimization of Drive Tests (MDT) feature first introduced in Rel-10 [20], allows operators to configure their UEs to report measurements with a specific periodicity to evaluate or improve network performance. This feature could be particularly useful for data gathering in the data-driven estimation approach.

This experiment uses the measurements recorded by the different devices, which go through the L1 and L3 filtering mentioned above. The measurements are obtained with a sampling rate of 500 ms, as shown in Table 2. To evaluate the variability of the measured RSRP, we performed a static over-the-air test of 6 minutes duration, where all phones were connected to the same serving cell and pointed towards the same orientation. The observed signal levels for the four phones are shown in Fig. 4. The mean μ and standard deviation σ of the measurements collected during the static test are also included in the figure. Different mean values are observed between the different phones, which further confirms the UE heterogeneity mentioned in Section III-A. It can also be seen that all mobile devices show a standard deviation of approximately 1 dB, generally lower than the results observed in [12] due to a stable environment during the test (no cars or moving objects surrounding). The static test affirms that RSRP recordings are stable and not significantly impacted by noise in the measurement acquisition. In practice, devices will show an offset between them due to implementation differences. In our analysis, this is degenerate to the offsets caused by the position and orientation of the phones/devices, i.e., a static mean offset.

IV. DATA-DRIVEN ESTIMATION TECHNIQUE

Considering the previous work in [7], this section summarizes how the recorded data is used to obtain the estimations. Using Fig. 5 as a reference, we explain how the estimation is built based on the values recorded by different UEs moving along the same route.

The routes of the two environments are split in a distance grid of J segments of 10 m length. This means that e.g., for the urban environment, the 3.3 km are split in $J = 330$ segments of 10 m. The serving cell traces recorded by each of the UEs in every run or loop are located in the corresponding distance grid. If UE_1 is taken as an example, it may correspond to e.g., the trace recorded in the urban environment by mobile device $S5_1$ in $Setup_A$ and $Loop_1$. Then UE_2 would correspond to the trace recorded by the same device, same setup, but $Loop_2$. The process would continue until the N traces are located in the distance grid, where N results from the following:

- Urban: 4 available phone devices in 3 different setups, where 3 loops of the route were driven. This results in a total of $N = 36$ recorded serving cell traces used to estimate the average signal level experienced by a UE driving along that urban route.
- Rural: 4 available phone devices in 3 different configurations or setups, where 4 runs (2 in each direction) of the route were driven. This results in a total of $N = 48$ recorded serving cell traces used to estimate the

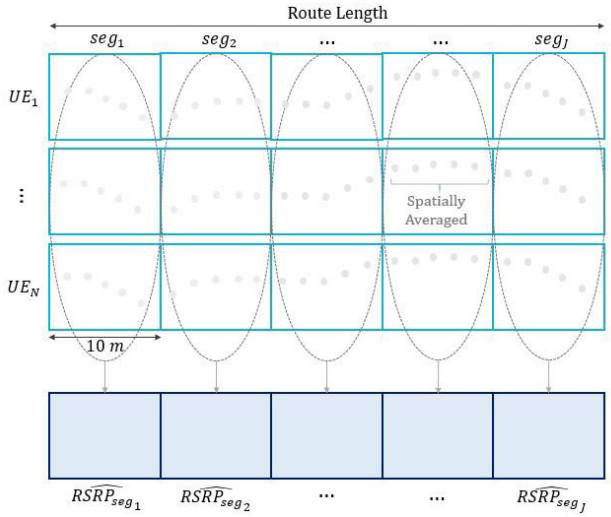

FIGURE 5. Data processing scheme. The different UE traces are located in a distance grid and averaged to obtain the estimation.

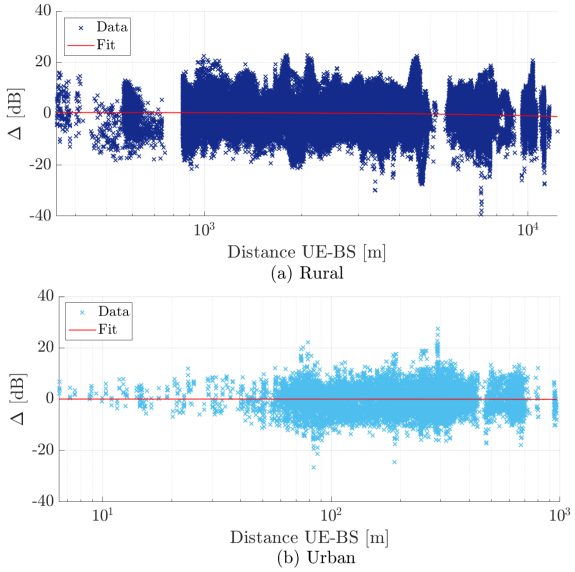

FIGURE 6. Estimation error versus UE-BS distance for the different scenarios: (a) rural and (b) urban.

average signal level experienced by a UE driving along that same rural route.

When a serving cell trace is located in the distance grid, multiple recorded samples are observed within a 10 m segment. The average number of samples recorded per segment depends on the driving speed and can be found in Table 2. As it is shown in Fig. 5, all the samples within the same grid segment are spatially averaged. This further averages fast fading effects previously mentioned in Section III-B: the selected 10 m segments fulfill the Lee criteria ($40\lambda = 6.6$ m) [24].

Once the N traces are organized in the distance grid, they are averaged to obtain an estimation. This is done on a segment basis, i.e. for each segment $j = 1, \ldots, J$ the values from all UEs $i = 1, \ldots, N$ are averaged, providing as a result an estimated value for each corresponding segment. The estimated RSRP value at a segment j is defined as the geometric average:

$$\widehat{RSRP}_{seg_j} = \frac{1}{N} \sum_{i=1}^{N} RSRP_{i,seg_j} \qquad \text{[dBm]} \quad (1)$$

where N takes the values defined above and $RSRP_{i,seg_j}$ is the RSRP value recorded by UE_i in segment j.

The RSRP measurements recorded by the UEs in a certain segment will be aggregated regardless of the cell that they are connected to. The main motivation behind this is that we aim to estimate the average signal level that any UE in that location would experience.

When aggregating measurements from different serving cells, it could be expected that UE-BS distance impacts the estimation error. The estimation error, shown in Fig. 6 and defined in Eq. (2), does not seem to be impacted by the UE-BS distance. This can be partially due to the cell selection and re-selection processes, which tend to minimize this effect. There is a high spread of the estimation error values regardless of the distance in both rural and urban scenarios.

In practice, the proposed data-driven approach requires measurement gathering from different users, which could be achieved through MDT. The accuracy of the estimations would be subject to factors such as Global Positioning System (GPS) inaccuracy, environment changes, or measurement system differences. While GPS inaccuracies are reduced by averaging every 10 m, but not otherwise considered in our analysis, measurement system differences are considered by including UE heterogeneity. Similarly, we include the unpredictable environment changes in the estimations by performing several different measurement rounds during the campaign. Additionally, keeping updated estimations and error distributions will require large database storage.

A. ESTIMATION ACCURACY AND PERFORMANCE COMPARISON

To evaluate the performance of the RSRP estimation algorithm, we compare the estimations to those obtained using empirical models and ray-tracing. Only urban environment data is used for the comparison due to the unavailability of 3D models and terrain elevation maps in the ray-tracing tool for the rural area.

As the performance metric, we use the estimation error calculated for each of the UEs and segments independently. For each UE_i ($i = 1, \ldots, N$) the estimation error $\Delta_{UE_{i,seg_j}}$ is calculated segment by segment as the difference between the recorded $RSRP_{UE_{i,seg_j}}$ value and the estimated $\widehat{RSRP}_{seg_j}$ value:

$$\Delta_{UE_{i,seg_j}} = RSRP_{UE_{i,seg_j}} - \widehat{RSRP}_{seg_j} \qquad \text{[dB]} \quad (2)$$

As was shown in [7], the distribution of the estimation error is uni-modal and can be well approximated with a

TABLE 3. Data-driven estimation errors based on UEs (before and after MIO correction) and scanner data.

	Rural Δ [dB]	Urban Δ [dB]
Before MIO Correction	6.3	4.9
After MIO Correction	4.9	3.6
Scanner	3.6	3.2

Gaussian $\mathcal{N}(0, \sigma)$. This suggests that the results obtained would remain unchanged regardless of the metric used for aggregation (mean, mode or median). Each UE presents an MIO with respect to the overall estimation, which, if corrected, can reduce the estimation error. Table 3 shows the overall estimation error with and without MIO correction for both urban and rural environments. Later in Section V-B we will introduce a technique for MIO correction to actually achieve the approximately 4 dB estimation error shown for MIO correction in Table 3.

For the comparison with empirical models and ray-tracing, Fig. 7 shows the recorded RSRP values versus distance to the serving BS together with the estimations based on these traditional approaches. The model parameters have been calibrated using measurement data or environment-specific parameters in each case. The data-driven estimations are not shown since they are cell agnostic and cannot be referenced to a specific site.

Table 4 shows the estimation error, as per Eq. (2), for all the studied techniques. In the case of the empirical and ray-tracing estimations, the estimated value is obtained for the corresponding Physical Cell ID (PCI) recorded by the UE during the measurement campaign, sample by sample. These estimations are then averaged on a segment basis to obtain a serving RSRP estimation at each segment. Further details on the respective approaches are:

1) EMPIRICAL MODELS

Two empirical models have been used for comparison: Okumura-Hata and 3GPP TR 38.901 for Urban Macro (UMa) environments. The operator provided network information (BS location, BS height, and BS radiated power), which was used to calculate the corresponding UE-BS distance for the specific serving cell and other relevant parameters for these empirical models. The UE assumed height is 1.5 m, and the center frequency is 1.8 GHz.

The Okumura-Hata Model [10] was developed using the results of very extensive measurements performed in different environments (urban and suburban). It is typically used by operators, which apply the necessary corrections to fine-tune the model to the specific physical environment under evaluation.

The 3GPP TR 38.901 standardized path loss model for the 3D Urban Macro (UMa) Line-Of-Sight (LOS) and Non-Line-of-Sight (NLOS) scenarios [25] is also used for comparison. The visibility conditions (LOS/NLOS) between the UE and the BS have been determined using the ray-tracing tool, and the corresponding equation from [25] is applied for each case.

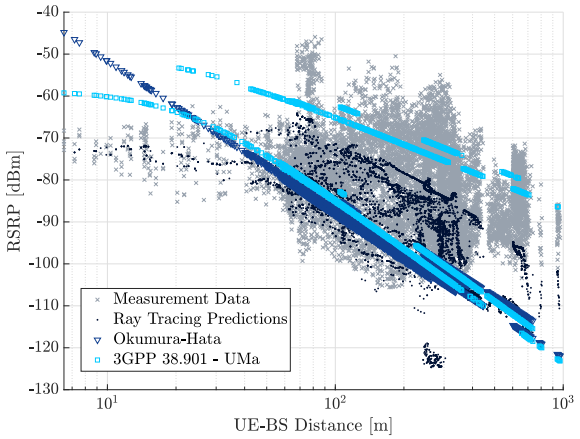

FIGURE 7. Comparison of measurement data with traditional estimation approaches in the urban scenario. LOS/NLOS conditions are considered.

TABLE 4. Comparison of data-driven approach estimation error with traditional techniques using urban scenario data.

Estimation Technique	Estimation Error [dB]
Data-Driven	4.9
Okumura-Hata	11.1
3GPP 38.901 UMa	9.3
Ray-Tracing	7.6

By observing Fig. 7 it can be seen that for a particular UE-BS distance the spread of the recorded measurements is high. The value estimated by the empirical models, which depends on the distance to the BS and visibility conditions, may not represent the signal level expected in a particular location. This is consistent with what is observed in Table 4, where the highest estimation errors are observed for the two empirical models. Both show estimation errors 4-6 dB higher than the observed when using the data-driven approach.

2) RAY-TRACING

A ray-tracing tool is used to obtain predictions for comparison with the data-driven approach [26]. The Dominant Path Model (DPM) is selected to compute the estimations, which calculates the dominant path between the transmitter and the receiver [27]. The 3D maps used in the tool have a 2.5 m spatial resolution. The predictions are further averaged on a 10 m radius in order to compare them with the other two approaches properly. The same is applied for the LOS/NLOS predictions, which are estimated every 2.5 m, and settled using a majority vote of LOS/NLOS conditions within a 10 m radius.

As observed in Fig. 7, ray-tracing shows more accurate estimations than the empirical models since it accounts for the specific physical environment surrounding the UE and not only the average area characteristics. This is also reflected in Table 4, where an 7.6 dB estimation error is observed. While this value is 2-4 dB lower than the one observed with the empirical techniques, it is still high.

The studied traditional techniques show worse performance than the data-driven approach. The data-driven estimation is based on real location-specific data and, therefore, provides a more accurate estimation than the traditional techniques of the signal level that the UE will perceive when driving along a route. However, a single estimated value is not representative enough, and each UE will observe a certain MIO with respect to the overall mean estimation. In the following sections, we study how the MIO can be predicted, corrected, and used to improve the accuracy of the estimation.

V. MEAN INDIVIDUAL OFFSET CORRECTION

A. PRE-SERVICE

Correcting the MIO in the pre-service stage would allow the network to perform more accurate estimations on the potential critical areas before the UE starts moving along the route. For that, the network should be able to predict the UE's MIO using relevant context information such as UE's placement (inside/outside the car), UE's orientation, or UE's pattern type, assuming these can be available.

1) UE ANTENNA ORIENTATION

The MIO for each UE in the rural (a) and urban environments (b) is shown in Fig. 8. As it can be observed, the offset remains constant between different runs or loops for the same phone-setup combination where the device is oriented towards the same direction. However, different offsets are observed between devices that are pointing in different directions. This illustrates the relevance of UE orientation to determine the MIO. A clear distinction can also be made between setups A-B and setup C. The phones were located inside the car in the latter, and the penetration loss due to the vehicle's structure caused the signal level to be much lower (7 dB on average) than the one experienced by the phones located in the car top carrier. This resulted in negative MIOs with respect to the overall estimation for all phones located inside the car. Therefore, it is reasonable to assume that another relevant factor impacting the MIO of a UE is its placement (inside/outside) in the car. However, that information would only allow identifying the sign of the MIO, but not the value of it, which seems to depend mainly on the UE orientation and driving direction (as previously shown in [7]).

2) UE ANTENNA PATTERN EFFECTS COMPENSATION

The consistency of the offset values observed among loops of each UE Fig. 8, as well as the different offsets for the multiple UEs, suggest that the orientation of the UE is potentially the main factor impacting the MIO. The signal level reaching the receiver will also be subjected to the device's effective antenna pattern, which is directional for all test phones (see Fig. 3).

Therefore, compensation for the antenna pattern effect could reduce the estimation error. The approach has been tested for the rural scenario data: the reduced interactions of the received signal with surrounding objects and the

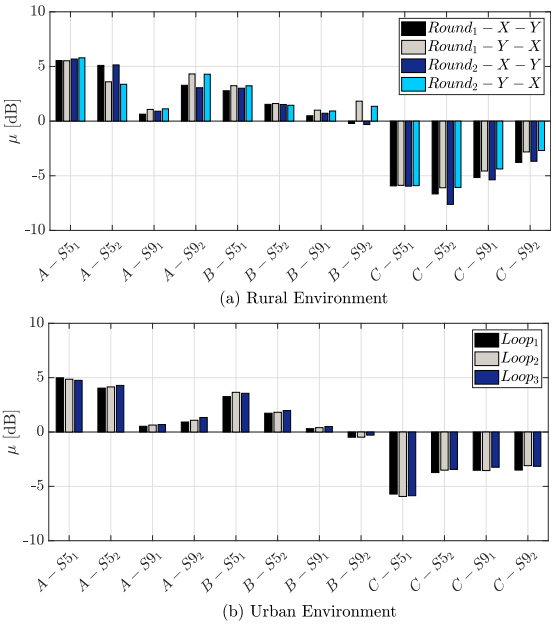

FIGURE 8. MIO with respect to the route estimation. (a) Results for each of the 48 UE traces in the rural environment and (b) for the 36 UE traces in the urban environment.

TABLE 5. Effective antenna pattern compensation effects on overall estimation error in the rural scenario.

	Δ [dB]
Before Antenna Pattern Compensation	5.1
After Antenna Pattern Compensation	4.7

dominance of LOS conditions simplifies the antenna pattern compensation in that environment. The angle of incidence α of the transmitted signal (from the BS) in the UE antenna pattern is calculated using the bearing angle of the serving BS (as recorded by the UE) with respect to the car direction. To account for possible inaccuracies in the calculation of α, the compensation is based on the average relative power shown in Fig. 3 within a $\pm 15°$ range in both azimuth and elevation directions.

Results in Table 5 show the overall estimation error Δ for the rural scenario when using setups A and B, before and after pattern compensation. As it can be observed, the antenna pattern compensation has a low impact, resulting in a reduction of 0.4 dB. Setup C is omitted due to the challenge of accounting for the vehicle blockage.

The antenna patterns were measured in an anechoic chamber, where the effects of the car structure or the car top carrier are not considered. Furthermore, the UE-BS distance is considerably high for the rural case, and possible signal interactions with the buildings in the path or ground reflections cannot be accounted for. Although deterministic compensation seems intractable, the stability of the estimation error between UEs oriented towards the same direction suggests that the antenna pattern effect is statistically included in the estimation error distribution. In the following section,

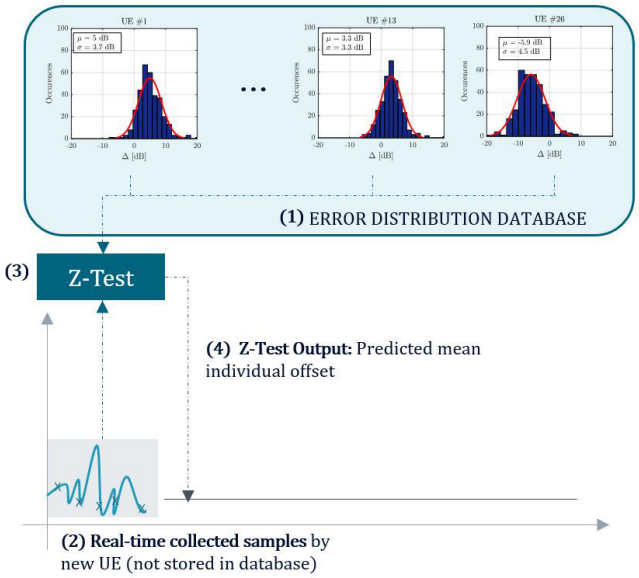

FIGURE 9. MIO correction procedure in the on-service stage. The moving UE estimation error samples are compared to the error distributions stored in the database and provide an estimation of the MIO.

we study an approach that exploits the stability of the estimation error of the UE traces recorded by devices oriented towards the same direction.

B. ON-SERVICE

The results in the previous section show that fully correcting the MIO in the pre-service stage is complex. In the following, we present how we use the estimation error characteristics and the observed error based on recorded RSRP during the on-service stage to correct the MIO. The main idea of this approach is to use the most recent information recorded by the UE that is moving along a particular route to predict the MIO that it will observe for the rest of the route.

We use the so-called z-test [28], which is a parametric hypothesis test that can be used to determine whether a set of samples belongs to a certain distribution. The test calculates the probability of observing as extreme a test result as the one observed (p-value), assuming that the null hypothesis is correct.

As shown in Fig. 9 (using notation $^{(\#)}$) this approach requires to maintain a database where estimation error distributions from previous UEs are stored $^{(1)}$. The distributions from each UE could be approximated by a normal distribution with the corresponding mean and standard deviation. Once the UE starts to move along the route, after a certain number of observed error samples $^{(2)}$, these are checked against the available distributions in the database. The z-test will provide the mean of the best-fit distribution $^{(4)}$ by accepting the distribution with the highest p-value.

To investigate this approach, we store $N - 0.25 * N$ distributions in the estimation error database and use the 25 % of the UE traces (i.e., 9 UE traces in the urban environment) for testing the algorithm. A set of 9 random traces is left out in every iteration until all the UEs have been tested. Fig. 10

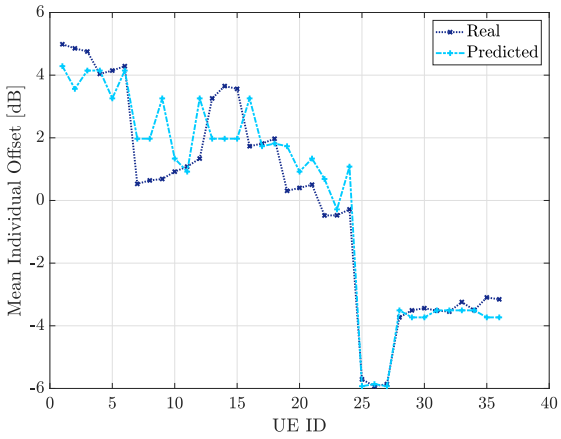

FIGURE 10. Necessary MIO corrections to improve estimation accuracy (light blue) and estimated on-service MIO corrections for all test UE traces in urban scenario (dark blue).

TABLE 6. Z-test results comparison with best performance observed in [7].

	Target Δ [dB] (known MIO)	Z-Test	
		Δ [dB]	d_{obs} [m]
Rural	4.9	5.1	100
Urban	3.6	3.7	300

shows the results obtained for urban scenario. The MIOs of the $N = 36$ UEs recorded in the urban environment are shown, as well as the predicted values using the z-test when observing 30 samples (equivalent to an observation distance of $d_{obs} = 300$ m). The MIO values can generally be accurately predicted. Table 6 shows a summary of the results obtained for both rural and urban scenarios. The table shows the overall results obtained when the MIO is known and corrected (Target Δ [dB]) and the results obtained when predicting and correcting the MIO using the z-test. The overall results when using the z-test for MIO estimation are reasonably close (maximum 0.2 dB difference) to the values using known offsets. Therefore, the MIO can be corrected using this technique as long as UEs with similar conditions/orientation have previously passed through the same route.

Table 6 also includes the required observation distance d_{obs}. In the urban environment a d_{obs} of 300 m is required, whereas for the rural scenario a d_{obs} of 100 m is sufficient. In the urban environment, an observation distance of 100 m reduces the overall estimation error from 4.9 dB to 4.1 dB, but a longer observation distance further decreases that value down to 3.7 dB. In the rural case, the error does not decrease regardless of the observation distance. This is most likely due to the stronger signal variations and higher dynamics that were observed in the rural scenario compared to the urban case.

VI. OUTAGE PROBABILITY ESTIMATION

As mentioned in Section II, signal level estimations can be used by the network to obtain information on the potential critical areas along the route, which are defined in terms of expected service availability and reliability. We further

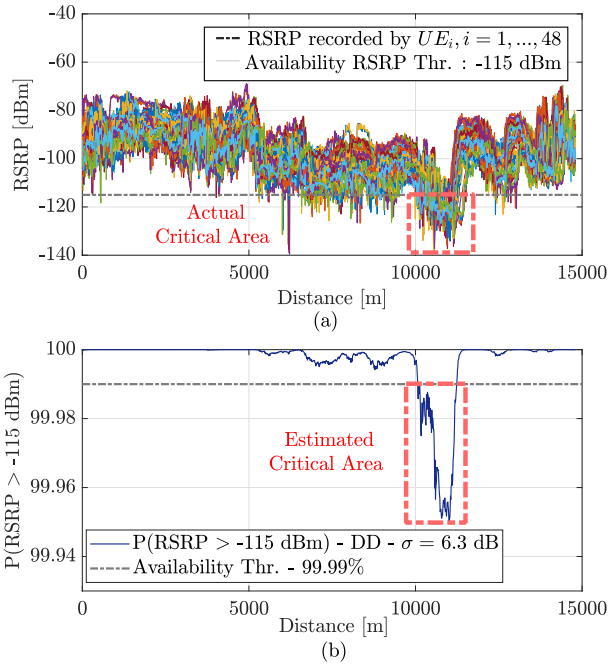

FIGURE 11. Service availability estimation example with rural environment data. (a) Actual RSRP values recorded by all 48 UEs used to build the estimation and (b) $P(RSRP > -115$ dBm) along the route, calculated based on the serving cell RSRP estimation.

define these QoS metrics and exemplify their use in the following. For a real reference, we focus on the specifications of the V2X services. Although the open literature claims that a requirement of 95 % reliability is enough for a safe communication [29], most of the use cases considered in the V2X 3GPP specifications [30] require a 99.99 % reliability, and that is the requirement we use for evaluation.

A. SERVICE AVAILABILITY

Service availability estimations are obtained by calculating the probability $P_{out,SA}$ that RSRP will drop below a certain threshold γ_{RSRP} along the route. For each segment, we provide an estimate of the average RSRP, $\widehat{RSRP}$. We know from Eq. (2) that the difference to the actual RSRP value, $RSRP - \widehat{RSRP}$, is Gaussian distributed with standard deviation sigma. Hence assuming, or conditioned on, $\widehat{RSRP}$ being the average RSRP, we calculate the outage probability as the one-sided p-value of the Gaussian distribution at the threshold value, i.e.:

$$\begin{aligned} P_{out,SA} &= P(RSRP < \gamma_{RSRP} | \overline{RSRP} = \widehat{RSRP}) \\ &= \Phi\left(\frac{\gamma_{RSRP} - \widehat{RSRP}}{\sigma}\right) \end{aligned} \quad (3)$$

where Φ is the cumulative distribution function of the standard normal distribution.

In Fig. 11 we show the availability estimation results along the rural route for a $\gamma_{RSRP} = -115$ dBm. This threshold is selected based on the observed intra-frequency mobility thresholds configured by the operator (which range between -115 dBm and -100 dBm in the 1800 MHz band). Fig. 11a shows the 48 recorded serving RSRP traces, while Fig. 11b presents the estimated availability for that route, where $P(RSRP > -115$ dBm), i.e. $1 - P(RSRP < -115$ dBm) is shown such that a 99.99 % threshold is used as a reference to declare a critical area for the selected use case. As it can be seen, the estimated potential critical areas visually match with the ones actually experienced by the UEs. Table 7 shows a summary of the service availability estimations performance. Service availability is evaluated for each segment in the distance grid. For the RSRP traces recorded by the different UEs, outage is declared in a grid segment if the recorded RSRP value in that segment is below γ_{RSRP}. For the estimated service availability, outage is declared in a grid segment if $P(RSRP > \gamma_{RSRP}) < 99.99$ % in that segment. Performance of service availability estimations is evaluated using the average over all UE traces of the following metrics [31]:

- **True Positive Rate (TPR)** or Hit Rate: Percentage of correctly estimated service availability outage segments in the grid. It is calculated as the number of correctly estimated outage segments - True Positives (TP) - over the number of actual outage segments (P).

$$TPR = \frac{TP}{P} \quad [\%] \quad (4)$$

- **True Negative Rate (TNR)** or Specificity: Percentage of correctly estimated service availability "safe" (non-outage) segments in the grid. It is calculated as the number of correctly estimated non-outage segments - True Negatives (TN) - over the number of actual non-outage segments (N).

$$TNR = \frac{TN}{N} \quad [\%] \quad (5)$$

- **False Negative Rate (FNR)** or Miss Rate: Complementary metric for TPR. Represents the number of missed outage areas.

$$FNR = 1 - TPR \quad [\%] \quad (6)$$

- **False Positive Rate (FPR)** or Fall-out: The complementary metric for TNR. Represents the number of "false alarms," i.e., the percentage of cases where a grid segment was incorrectly estimated as outage area. False positives would lead to a situation where countermeasures are initiated to solve a critical situation that does not exist.

$$FPR = 1 - TNR \quad [\%] \quad (7)$$

Other metrics that are typically used to evaluate classification techniques were not included as they were considered to be misleading in the purpose of this context. Accuracy is typically used to summarize the performance of the estimations, as it represents the rate of correct estimations (positive and negative). However, for the case under evaluation, where the number of actual positives is much lower than the number of actual negatives (unbalanced dataset), accuracy presented

TABLE 7. Average performance metrics for RSRP-based service availability estimations.

		TPR (Hit Rate) [%]	TNR (Specificity) [%]	FNR (Miss Rate) [%]	FPR (Fall-out) [%]
Rural γ_{RSRP} = -115 dBm	**Data-Driven** *Pre-Service*	85.2	95.7	14.8	4.3
	Data-Driven *On-Service*	74.3	97.1	25.7	2.9
Urban γ_{RSRP} = -100 dBm	**Okumura-Hata**	100	4.3	0	95.7
	3GPP 38.901	70	62.4	30	37.6
	Ray-Tracing	63.1	69.4	36.9	30.6
	Data-Driven *Pre-Service*	93.8	83.8	6.2	16.2
	Data-Driven *On-Service*	99.5	89.5	0.5	10.5

very high values (above 90 % for the data-driven approach) and was considered to be non-representative of the estimation performance. F1-Score, on the other hand, is typically used for unbalanced datasets and is calculated such that the cost of false positives and false negatives is equally significant for performance evaluation [32]. This metric presented low values (below 65 %) due to the low number of critical areas for some of the UEs.

Results in Table 7 show the mean value of the metrics in Eqs. (4-7) over all UEs. For rural environments, the pre-service stage estimations present high TPR and TNR, indicating that most outage and non-outage areas are correctly estimated. A trade-off is observed in the on-service stage, where the MIO corrections cause a decrease in the TPR and an increase in the TNR.

Another example of service availability estimation is shown in Fig. 12, where urban data is used to compare the estimation of critical areas when using the data-driven approach in comparison to the traditional estimation techniques. To show the accuracy of the estimations, the availability threshold is raised in this scenario to -100 dBm as higher reliability should be considered in higher population density areas. As shown in Fig. 12b and in Table 7, the higher the signal level estimation error, the lower is the accuracy of the estimated critical areas. Using the Okumura-Hata model RSRP estimations results in a very inaccurate estimation of the potential critical areas. Since the full route is declared critical the TPR is 100 %. However, it also presents a very high FPR of 96 %. The 3GPP model estimations show lower FPR than the Okumura-Hata, but still considerably high (38 %). Similar results are observed for the ray-tracing estimations that show a TPR of 63 % and an FPR of 31 %. The data-driven approach provides an average TPR of 94 % in the pre-service stage while maintaining a relatively low FPR (16 %). This shows how the data-driven signal level estimation technique provides better results than traditional techniques when the network aims to obtain in-advance information about the expected service availability along the path.

To further show the benefits of using the data-driven estimations against other traditional techniques, we show in

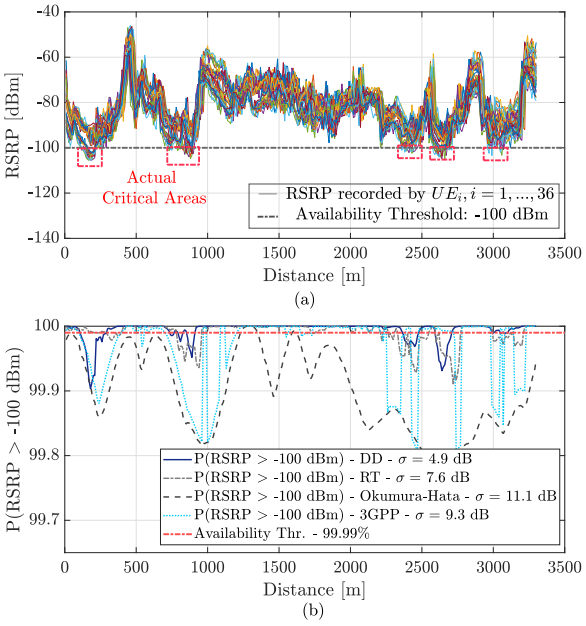

FIGURE 12. Service availability estimation example with urban environment data. (a) Actual RSRP values recorded by all 36 UE traces used to build the estimation and (b) $P(RSRP > -100$ dBm) obtained when using the estimations provided by the different studied RSRP estimation approaches.

Table 8 the reliability margin (RM) that needs to be considered to guarantee a certain reliability requirement when using the different estimation techniques. The values in the table show that the reliability margin highly decreases when using the data-driven approach. For a 99.99 % reliability requirement, the Okumura-Hata estimations show an RM of almost 28 dB, whereas the data-driven approach reduces the margin to 8 dB in the on-service stage. Higher reliability requirements are not considered in the table as the RM values would be on the limit of what could be practically useful for the purpose of the estimations considered in this article.

In Fig. 13 we show the effect that MIO correction has on the estimation of critical areas in the on-service stage. Three UEs were used as an example, one from each of the setups. For each UE, the z-test was used to obtain the corresponding MIO

TABLE 8. Reliability margin (RM) for different reliability requirements (with $\gamma_{RSRP} = -100$ dBm).

	90 %	95 %	99.99 %
Okumura-Hata	15.2	19.5	27.6
3GPP TR 38.901	12.3	15.7	22.3
Ray-Tracing	10	12.8	18.1
Data-Driven Pre-service	6.2	8	11.3
Data-Driven On-service	4.6	5.9	8.3

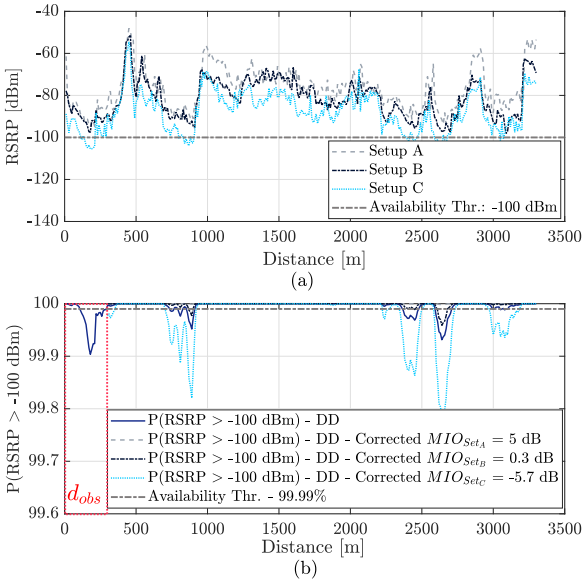

FIGURE 13. Service availability estimation example with urban environment data. (a) Actual RSRP values recorded by 3 example UEs (from setups A, B, C) and (b) $P(RSRP > -100$ dBm) along the route, for the pre-service estimation of all UEs in that path and the on-service estimations for the individual example UEs.

estimation. After an observation distance of $d_{obs} = 300$ m, the serving RSRP estimation was corrected according to the estimated MIO, and the probability of RSRP being below -100 dBm was recalculated. In Fig. 13a the actual serving RSRP traces recorded by each of the three UEs are shown. Fig. 13b shows $P(RSRP > -100$ dBm) in the pre-service stage (valid for any UE planning to move through the same path) and the corrected on-service probability for each of the 3 example UEs (UE-specific estimation). The setup A UE, with positive MIO with respect to the overall estimation, has lower probabilities of dropping below the threshold than initially estimated. There are no critical areas estimated after MIO correction, which matches with the recorded values for that UE (never below -100 dBm). For Setup C UE, with generally lower signal levels due to vehicle blockage, the estimated probabilities of the serving signal level dropping below the threshold are higher than estimated in the pre-service stage, representing well the actual signal levels experienced by that user. The results for on-service stage performance in the urban environment in Table 7 show that on average, TPR increases to 99 % with respect to 94 % obtained in the pre-service stage, and TNR increases up to 89 % compared to the previous 84 %.

B. SERVICE RELIABILITY

To estimate service reliability we first estimate SIR:

$$\widehat{SIR} = \frac{\hat{S}}{\hat{I}} = \frac{\widehat{RSRP_{SC}}}{\sum_{j=1}^{NC} \widehat{RSRP_j} \cdot \delta} \quad [\text{dB}] \quad (8)$$

$\widehat{RSRP_{SC}}$ is the RSRP estimation of the serving cell, $\widehat{RSRP_j}$ is the estimation of the $j = 1, \ldots, NC$ neighboring cells and δ is a model for the impact of the traffic load. A maximum of $NC = 3$ strongest neighbors, when available, are used to calculate SIR.

As in Eq. (2), since $RSRP - \widehat{RSRP}$ is Gaussian with zero mean we can view the linear value of the estimator $\widehat{RSRP}$ as a log-normal random variable whose logarithmic mean and standard deviation is respectively the prediction $\widehat{RSRP}$ and σ. This is true for both serving and interfering signals. The interference sum will be approximately log-normal, statistics of which can be calculated numerically by the Schwarz & Yeh algorithm [33]. The same algorithm, with some extensions for correlated signals, can be used to calculate the logarithmic mean and standard of the SIR [34] which is also approximately log-normal. Assuming a correlation coefficient of 0.5 [35] between signals of the serving and the interfering cells we use this framework to evaluate the probability $P(SIR < \gamma_{SIR})$.

Fig. 14b shows the reliability estimation results when considering low, medium and high load (10 %, 30 % and 60 %, respectively) for $\gamma_{SIR} = -3$ dB. In Fig. 14c a color map is used to plot the results for medium load with that same threshold in the urban scenario. The corresponding performance metrics in Table 9 show a TPR of 88 % and a FPR of 41 %, with a mean F1-score of 16 %. With the on-service stage corrections using MIO correction for the serving cell, results show the same trade-off TPR/TNR above-mentioned. For the rural environment, the values follow the same trend.

The presented results are sensitive to different network traffic load, critical thresholds, and correlation coefficients between the serving cell and the interfering neighbors. For most cases, MIO correction reduces TPR and increases TNR, indicating a trade-off between missing outage areas and initiating actions against non-existent ones. Failing to estimate an outage area poses a risk to the service reliability, which is crucial for mission-critical services. On the other hand, estimating non-existent critical areas may lead to a misuse of network resources. On that basis, MIO correction in the on-service stage is beneficial for outage areas estimation. However, initiating MIO correction in the on-service stage may depend on the service priorities, i.e. prioritization of outage area detection or more efficient resource utilization. Furthermore, service reliability could also benefit from the on-service MIO corrections due to the availability of actual load values, which could be adjusted individually for each corresponding neighbor.

TABLE 9. Average performance metrics for SIR-based service reliability estimations ($\delta = 30$ %).

		TPR (Hit Rate) [%]	TNR (Specificity) [%]	FNR (Miss Rate) [%]	FPR (Fall-out) [%]
Rural γ_{SIR} = -3 dB	**Data-Driven** *Pre-Service*	72.4	62.4	27.6	37.6
	Data-Driven *On-Service*	65	72.3	35	27.7
Urban γ_{SIR} = -3 dB	**Data-Driven** *Pre-Service*	88.2	58.8	11.8	41.2
	Data-Driven *On-Service*	77	68.7	23	31.3

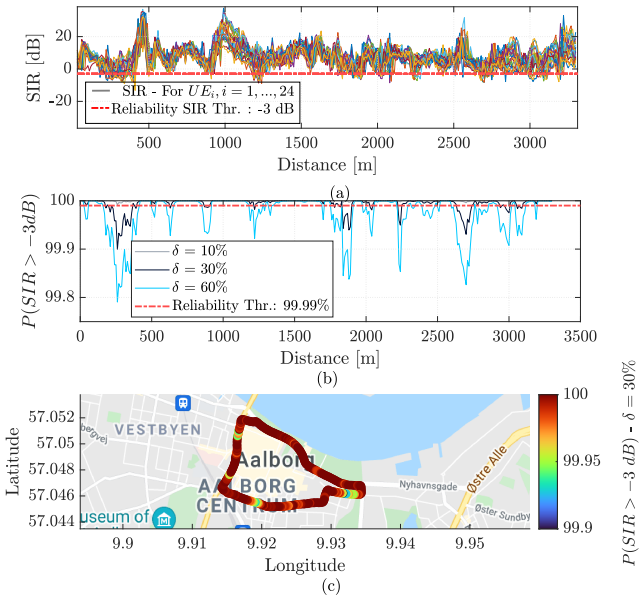

FIGURE 14. Service reliability estimation example with urban environment data. (a) SIR values calculated using recorded RSRP values from serving and neighboring cells for all of the 24 UEs used and assuming average medium load, (b) estimated probability $P(SIR > -3$ dB) for low, medium and high load and (c) same results at medium load in a color map.

VII. CONCLUSION

In this article, we use experimental data recorded during an extensive LTE measurement campaign in rural and urban environments to show that the signal level that a UE will experience along a route can be estimated by aggregating measurements recorded by UEs that have previously passed through that same route.

First, we show how this approach provides an estimation error of 5-6 dB, improving the estimation error obtained using traditional estimation techniques such as empirical models or ray-tracing by 3-6 dB. We show how identifying the MIO of each UE with respect to the overall estimation, using a technique that exploits the estimation error experienced by previous UEs, further reduces the overall RSRP estimation error to approximately 4 dB.

Lastly, we use the signal level estimations to calculate service outage probability in terms of availability (RSRP-based) and reliability (SIR-based). The data-driven approach shows improved accuracy in outage areas estimation with respect to traditional techniques, detecting a minimum of 70 % of the outage areas with less than 30 % of false alarms. This approach allows providing the network with in-advance information on the expected service conditions in a specific route where the UE is planning to move and can be used by the network to make a decision of whether it is safe for the UE to start the service or it should re-plan the route when possible. Furthermore, we show how using context information during the service can improve the overall accuracy of the service availability and reliability estimations, which the network may use to take in-advance countermeasures for upcoming signal and QoS drops, respectively.

REFERENCES

[1] *5G; Management and orchestration; 5G end to end Key Performance Indicators (KPI)*, Standard 3GPP TS 28.554 version 15.2.0 Release 15, 2019.

[2] J. Riihijarvi and P. Mahonen, "Machine learning for performance prediction in mobile cellular networks," *IEEE Comput. Intell. Mag.*, vol. 13, no. 1, pp. 51–60, Feb. 2018, doi: 10.1109/MCI.2017.2773824.

[3] L. Alho, A. Burian, J. Helenius, and J. Pajarinen, "Machine learning based mobile network throughput classification," in *Proc. IEEE Wireless Commun. Netw. Conf. (WCNC)*, Mar. 2021, pp. 1–6, doi: 10.1109/WCNC49053.2021.9417365.

[4] T. Linget, "White paper: Making 5G proactive and predictive for the automotive industry," 5G Automot. Assoc., Brussels, Belgium, White Paper, Jan. 2020.

[5] *Interface for Data Exchange between MNOs and the UTM Ecosystem: Network Coverage Service Definition*, document v1.00. ACJA, GSMA and GUTMA Approved Version, Feb. 2021.

[6] *Evolved Universal Terrestrial Radio Access (E-UTRA); Physical Layer Measurements*, Standard 3GPP TS 36.214 Version 9.1.0 Release 9, 2013.

[7] M. Lopez, T. B. Sorensen, I. Z. Kovacs, J. Wigard, and P. Mogensen, "Experimental evaluation of data-driven signal level estimation in cellular networks," in *Proc. IEEE 94th Veh. Technol. Conf. (VTC-Fall)*, Sep. 2021, pp. 1–6, doi: 10.1109/VTC2021-Fall52928.2021.9625559.

[8] V. Raida, P. Svoboda, M. Koglbauer, and M. Rupp, "On the stability of RSRP and variability of other KPIs in LTE Downlink–An open dataset," in *Proc. GLOBECOM - IEEE Global Commun. Conf.*, Dec. 2020, pp. 1–6, doi: 10.1109/GLOBECOM42002.2020.9348145.

[9] J. Walfisch and H. L. Bertoni, "A theoretical model of UHF propagation in urban environments," *IEEE Trans. Antennas Propag.*, vol. AP-36, no. 12, pp. 1788–1796, Dec. 1988, doi: 10.1109/8.14401.

[10] *Okumura-Hata Propagation Prediction Model for UHF Range, in the S*, document ITU-R Recommendation P. 529-2., ITU, Geneva, Switzerland, 1995, pp. 5–7.

[11] Z. Yun and M. F. Iskander, "Ray tracing for radio propagation modeling: Principles and applications," *IEEE Access*, vol. 3, pp. 1089–1100, 2015, doi: 10.1109/ACCESS.2015.2453991.

[12] M. Toril, V. Wille, S. Luna-Ramirez, M. Fernandez-Navarro, and F. Ruiz-Vega, "Characterization of radio signal strength fluctuations in road scenarios for cellular vehicular network planning in LTE," *IEEE Access*, vol. 9, pp. 33120–33131, 2021, doi: 10.1109/ACCESS.2021.3060995.

[13] F. Sohrabi and E. Kuehn, "Construction of the RSRP map using sparse MDT measurements by regression clustering," in *Proc. IEEE Int. Conf. Commun. (ICC)*, May 2017, pp. 1–6, doi: 10.1109/ICC.2017.7997073.
[14] A. Ghasemi, "Data-driven prediction of cellular networks coverage: An interpretable machine-learning model," in *Proc. IEEE Global Conf. Signal Inf. Process. (GlobalSIP)*, Nov. 2018, pp. 604–608, doi: 10.1109/GlobalSIP.2018.8646338.
[15] J. Thrane, B. Sliwa, C. Wietfeld, and H. L. Christiansen, "Deep learning-based signal strength prediction using geographical images and expert knowledge," in *Proc. GLOBECOM IEEE Global Commun. Conf.*, Dec. 2020, pp. 1–6, doi: 10.1109/GLOBECOM42002.2020.9322089.
[16] S. I. Popoola, E. Adetiba, A. A. Atayero, N. Faruk, and C. T. Calafate, "Optimal model for path loss predictions using feed-forward neural networks," *Cogent Eng.*, vol. 5, no. 1, Jan. 2018, Art. no. 1444345, doi: 10.1080/23311916.2018.1444345.
[17] M. Ayadi, A. B. Zineb, and S. Tabbane, "A UHF path loss model using learning machine for heterogeneous networks," *IEEE Trans. Antennas Propag.*, vol. 65, no. 7, pp. 3675–3683, Jul. 2017, doi: 10.1109/TAP.2017.2705112.
[18] E. Ostlin, H.-J. Zepernick, and H. Suzuki, "Macrocell path-loss prediction using artificial neural networks," *IEEE Trans. Veh. Technol.*, vol. 59, no. 6, pp. 2735–2747, Jul. 2010, doi: 10.1109/TVT.2010.2050502.
[19] *Architecture Enhancements for 5G System (5GS) to support Network Data Analytics Services*, Standard 3GPP TS 23.288, v17.0.0, Mar. 2021.
[20] *UTRA and E-UTRA; Radio Measurement Collection for Minimization of Drive Tests (MDT)*, Standard 3GPP TS 37.320 v16.4.0, 2018.
[21] (2019). *R&S Test Equipment Information. TSME Radio Network Scanner and QualiPoc Android Test Devices Manual*. [Online]. Available: https://www.rohde-schwarz.com/dk/product/
[22] (Mar. 25, 2020). *StarGate 24 Anechoic Chamber. Satimo Manual*. [Online]. Available: https://www.mvg-world.com/en/products/antenna-measurement/multi-probe-systems/sg-24
[23] D. Lopez-Perez, I. Guvenc, and X. Chu, "Mobility management challenges in 3GPP heterogeneous networks," *IEEE Commun. Mag.*, vol. 50, no. 12, pp. 70–78, Dec. 2012, doi: 10.1109/MCOM.2012.6384454.
[24] W. Lee and Y. Yeh, "On the estimation of the second-order statistics of log normal fading in mobile radio environment," *IEEE Trans. Commun.*, vol. COM-22, no. 6, pp. 869–873, Jun. 1974, doi: 10.1109/TCOM.1974.1092290.
[25] *Technical Specification Group Radio Access Network; Study on Channel Model for Frequencies From*, Standard 3GPP TR 38.901 0.5 to 100 GHz (Release 16) V16.1.0, Dec. 2019.
[26] *WinProp Manual, Version*, Altair Hyperworks, Troy, MI, USA, Jan. 2018.
[27] R. Wahl, G. Wölfle, P. Wertz, P. Wildbolz, and F. Landstorfer, "Dominant path prediction model for urban scenarios," in *Proc. 14th IST Mobile Wireless Commun. Summit*, Dresden, Germany, 2005, pp. 1–5.
[28] L. J. Kitchens, *Basic Statistics and Data Analysis*. Duxbury, MA, USA: Cengage Learn., 2003.
[29] G. Pocovi, M. Lauridsen, B. Soret, K. I. Pedersen, and P. Mogensen, "Automation for on-road vehicles: Use cases and requirements for radio design," in *Proc. IEEE 82nd Veh. Technol. Conf. (VTC-Fall)*, Sep. 2015, pp. 1–5.
[30] *Study on Enhancement of 3GPP Support for 5G V2X Services*, Standard 3GPP TR 22.886 Version 16.2.0 Release 16, 2018.
[31] Ferri, César, José Hernández-Orallo, and R. Modroiu, "An experimental comparison of performance measures for classification," *Pattern Recognit. Lett.*, vol. 30, no. 1, pp. 27–38, 2009, doi: 10.1016/j.patrec.2008.08.010.
[32] J. Brownlee, *Imbalanced Classification With Python: Better Metrics, Balance Skewed Classes, Cost-Sensitive Learning*. Montpelier, VT, USA: Machine Learning Mastery, 2020.
[33] S. C. Schwartz and Y. S. Yeh, "On the distribution function and moments of power sums with log-normal components," *Bell Syst. Tech. J.*, vol. 61, no. 7, pp. 1441–1462, Sep. 1982, doi: 10.1002/j.1538-7305.1982.tb04353.x.
[34] T. B. Sørensen, "Intelligent distributed antenna systems (IDAS); Assessment by measurement and simulation," Ph.D. dissertation, Dept. Electron. Syst., Aalborg Univ., Aalborg, Denmark, Feb. 2002.
[35] T. B. Sørensen, "Slow fading cross-correlation against azimuth separation of base stations," *Electron. Lett.*, vol. 35, no. 2, pp. 127–129, 1999, doi: 10.1049/el:19990085.

MELISA LÓPEZ (Graduate Student Member, IEEE) received the B.Sc. and M.Sc. degrees in telecommunications engineering from the Universitat Politécnica de Catalunya, Spain, in 2016 and 2018, respectively. She is currently pursuing the Ph.D. degree in wireless communications with Aalborg University, Denmark. Her research interests include radio propagation, field measurements, and cellular-based connectivity for mission-critical communications.

TROELS B. SØRENSEN received the M.Sc.E.E. degree, in 1990, and the Ph.D. degree in wireless communications from Aalborg University, in 2002. He worked with type approval test methods as part of ETSI standardization activities. Since 1997, he has been with Aalborg University, where he is currently an Associate Professor with the Section for Wireless Communication Networks. He has successfully supervised more than 15 Ph.D. students, and published more than 120 journal articles and conference papers. His research interests include cellular network performance and evolution, radio resource management, propagation characterization, and related experimental activities.

ISTVÁN Z. KOVÁCS (Member, IEEE) received the B.Sc. degree from the "Politehnica" Technical University of Timişoara, Romania, in 1989, the M.Sc.E.E. degree from the École Nationale Supérieure des Télécommunications de Bretagne, France, in 1996, and the Ph.D.E.E. degree in wireless communications from Aalborg University, Denmark, in 2002. He is currently a Senior Research Engineer at Nokia, Aalborg, Denmark, where he conducts standardization research on machine learning-driven radio resource management and on radio connectivity enhancements for non-terrestrial and aerial vehicle communications, in LTE and 5G networks.

JEROEN WIGARD received the M.Sc. degree in electrical engineering from Technische Universiteit Delft, The Netherlands, in 1995, and the Ph.D. degree on the topic of handover algorithms and frequency planning in frequency hopping GSM networks from Aalborg University, Denmark, in 1999. He joined Nokia, Aalborg, Denmark, where he worked on radio resource management related topics for 2G, 3G, 4G, and 5G. He is currently with Nokia Standards, and leads a research project for 5G standardization related to UAVs, and non terrestrial networks (NTN). He has authored or coauthored over 100 journal articles and conference papers and is an inventor of more than 100 patents applications.

PREBEN MOGENSEN received the M.Sc. and Ph.D. degrees from Aalborg University, in 1988 and 1996, respectively. Since 1995, he has been a part-time Associate with Nokia. Since 2000, he has been a Full Professor with Aalborg University, where he is currently leading the Wireless Communication Networks Section. He is also a Principal Scientist with Nokia Bell Labs and a Nokia Bell Labs Fellow. He has coauthored over 400 articles in various domains of wireless communication. His Google Scholar H-index is 61. His current research interests include the 5G industrial IoT and technology components towards 6G.